Formation and Photoinduced Electron Transfer in Porphyrin- and Phthalocyanine-Bearing N-Doped Graphene Hybrids Synthesized by Click Chemistry

Luis M. Arellano,[a] Habtom B. Gobeze,[b] Youngwoo Jang,[b] Myriam Barrejón,[c] Concepción Parejo,[d] Julio C. Álvarez,[d] María J. Gómez-Escalonilla,[a] Ángela Sastre-Santos,*[d] Francis D'Souza,*[b] and Fernando Langa*[a]

Abstract: Graphene doped with heteroatoms such as nitrogen, boron, and phosphorous by replacing some of the skeletal carbon atoms is emerging as an important class of two-dimensional materials as it offers the much-needed bandgap for optoelectronic applications and provides better access for chemical functionalization at the heteroatom sites. Covalent grafting of photosensitizers onto such doped graphenes makes them extremely useful for light-induced applications. Herein, we report the covalent functionalization of N-doped graphene (NG) with two well-known electron donor photosensitizers, namely, zinc porphyrin (ZnP) and zinc phthalocyanine (ZnPc), using the simple click chemistry approach. Covalent attachment of ZnP and ZnPc at the N-sites of NG in NG—ZnP and NG—ZnPc hybrids was confirmed by using a range of spectroscopic, thermogravimetric and imaging techniques. Ground- and excited-state interactions in NG—ZnP and NG—ZnPc were monitored by using spectral and electrochemical techniques. Efficient quenching of photosensitizer fluorescence in these hybrids was observed, and the relatively easier oxidations of ZnP and ZnPc supported excited-state charge-separation events. Photoinduced charge separation in NG—ZnP and NG—ZnPc hybrids was confirmed by using the ultrafast pump-probe technique. The measured rate constants were of the order of 10^{10} s,$^{-1}$ thus indicating ultrafast electron transfer phenomena.

Introduction

Graphene, a novel nanomaterial comprising a single sheet of carbon atoms packed in a hexagonal lattice[1–4] has emerged as one of the most actively researched materials for applications in

[a] Dr. L. M. Arellano, Dr. M. J. Gómez-Escalonilla, Prof. F. Langa
Universidad de Castilla-La Mancha
Instituto de Nanociencia, Nanotecnología y Materiales Moleculares (IN-AMOL)
Avda. Carlos III, s/n, 45071-Toledo (Spain)
E-mail: Fernando.Langa@uclm.es

[b] Dr. H. B. Gobeze, Y. Jang, Prof. F. D'Souza
Department of Chemistry and Materials Science and Engineering
University of North Texas, Denton, TX 76203-5017 (USA)
E-mail: francis.dsouza@unt.edu

[c] Dr. M. Barrejón
Neural Repair and Biomaterials Laboratory
Hospital Nacional de Parapléjicos (SESCAM)
Finca la Peraleda s/n, 45071 Toledo (Spain)

[d] Dr. C. Parejo, Dr. J. C. Álvarez, Prof. Á. Sastre-Santos
Área de Química Orgánica, Instituto de Bioingeniería
Universidad Miguel Hernández
Avda. de la Universidad, s/n, Elche 03202 (Spain)
E-mail: asastre@umh.es

🖥 Supporting information for this article is available on the WWW under https://doi.org/10.1002/chem.202200254

the areas of energy conversion and storage, electrocatalysis, sensors and electronics.[5–11] Controlled chemical doping of heteroatoms such as nitrogen, sulfur, and boron has provided a means of tailoring the properties of graphene, to match those of heteroatom-doped nanotubes, thereby broadening its scope.[12] Among the heteroatom-doped graphenes synthesized, nitrogen-doped graphene (NG), which contains three common bonding configurations within the carbon lattice, namely, quaternary N, pyridinic N and pyrrolic N[13] exhibits properties different from those of pristine graphene including bandgap tuning.

For functionalization purposes, NG offers a significant advantage as it can be conveniently functionalized at the pyrrolic nitrogen sites using established chemical techniques. Recently, we reported a chemical functionalization method that involves the reaction of an alkyl halide at the pyrrolic N.[13] Two donor-acceptor hybrids, namely, NG—C_{60} and NG-perylene diimide (PDI), in which electron-deficient C_{60}[14] and PDI[15] serve as electron acceptors, were successfully synthesized using this approach. Subsequently, photoinduced charge separation leading to NG$^{•+}$—$C_{60}^{•-}$ and NG$^{•+}$—PDI$^{•-}$ states was confirmed using time-resolved pump-probe techniques. In other words, NG is acting as an electron donor in these systems.[14,15] However, a literature search showed that the ability of NG to act as an electron acceptor under light illumination conditions has yet to be established. This becomes especially important for the application of NG in light-energy and light-to-fuel conversion and other catalytic applications.[16] With this in mind, in the

Chem. Eur. J. **2022**, 28, e202200254 (1 of 10)

© 2022 The Authors. Chemistry - A European Journal published by Wiley-VCH GmbH

Chemistry–A European Journal

Research Article
doi.org/10.1002/chem.202200254

Chemistry Europe
European Chemical
Societies Publishing

present study, we have functionalized NG with two well-known electron donors, namely, zinc porphyrin (ZnP)[17] and zinc phthalocyanine (ZnPc).[18,19] Additionally, zinc porphyrin has been functionalized to carry charge-stabilizing triphenylamine entities at the macrocycle periphery ZnP(TPA)₃ (Figure 1), and ZnPc has been functionalized with tert-octylphenoxy groups at the peripherical positions to make it a better electron donor while improving solubility.[20] ZnP(TPA)₃ also presents an alkyne group and ZnPc-N₃ an azido group in order to carry out highly facile click chemistry reaction to attach the maximum numbers of electron donor entities while also improving the solubility of these hybrids systems in common solvents (Figure 1). Both NG—ZnP(TPA)₃ (**1**) and NG—ZnPc (**2**) hybrids are characterized using a variety of spectral, imaging and electrochemical techniques and the occurrence of photoinduced electron transfer is demonstrated using ultrafast transient absorption technique.

Results and Discussion

Commercial nitrogen-doped graphene (NG: http://www.time-snano.com) was first exfoliated in *N*-methyl-2-pyrrolidone (NMP; see the Experimental Section for details). This gave a dispersion of few-laye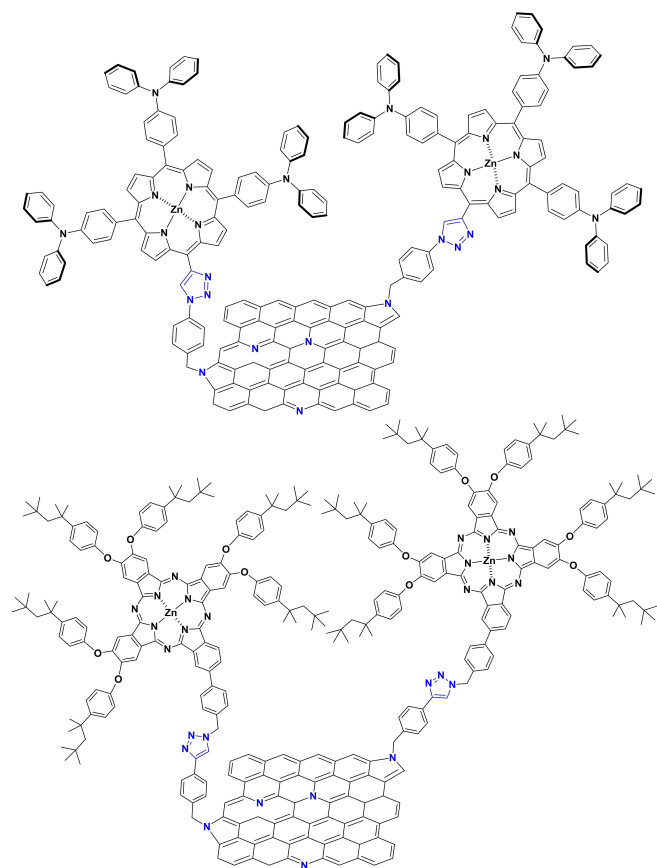r graphene sheets (3 or 4 layers). The Raman spectrum (laser excitation at 532 nm) of exfoliated NG shows the characteristic D and G bands for graphitic materials at 1353 and 1586 cm,$^{-1}$ respectively (Figure 2a). As previously reported for nitrogen-doped graphene,[14,15] the existence of significant defects related to the presence of nitrogen within the graphitic network increased the intensity of the D band and broaden the Raman bands, thus hampering the observation of any difference after the functionalization.

Atomic force microscopy (AFM; Figure 2b) of this material revealed an average thickness of 3 nm corresponding to few-layer graphene (3 or 4 layers). In addition, thinner sheets with an average height of about 1.4 nm corresponding to single-layer graphene were observed, in line with the Raman data (Figure 2a). Finally, TEM analysis showed the presence of agglomerated few-layer graphene sheets with dimensions of several hundred nanometers and high crystallinity (Figure 2c).
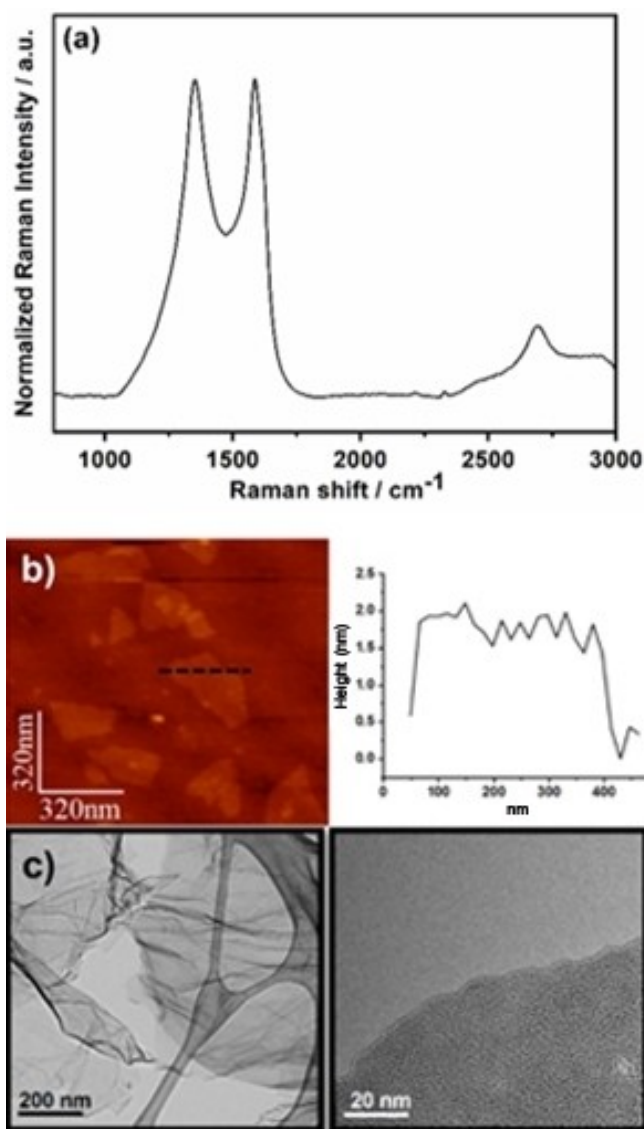

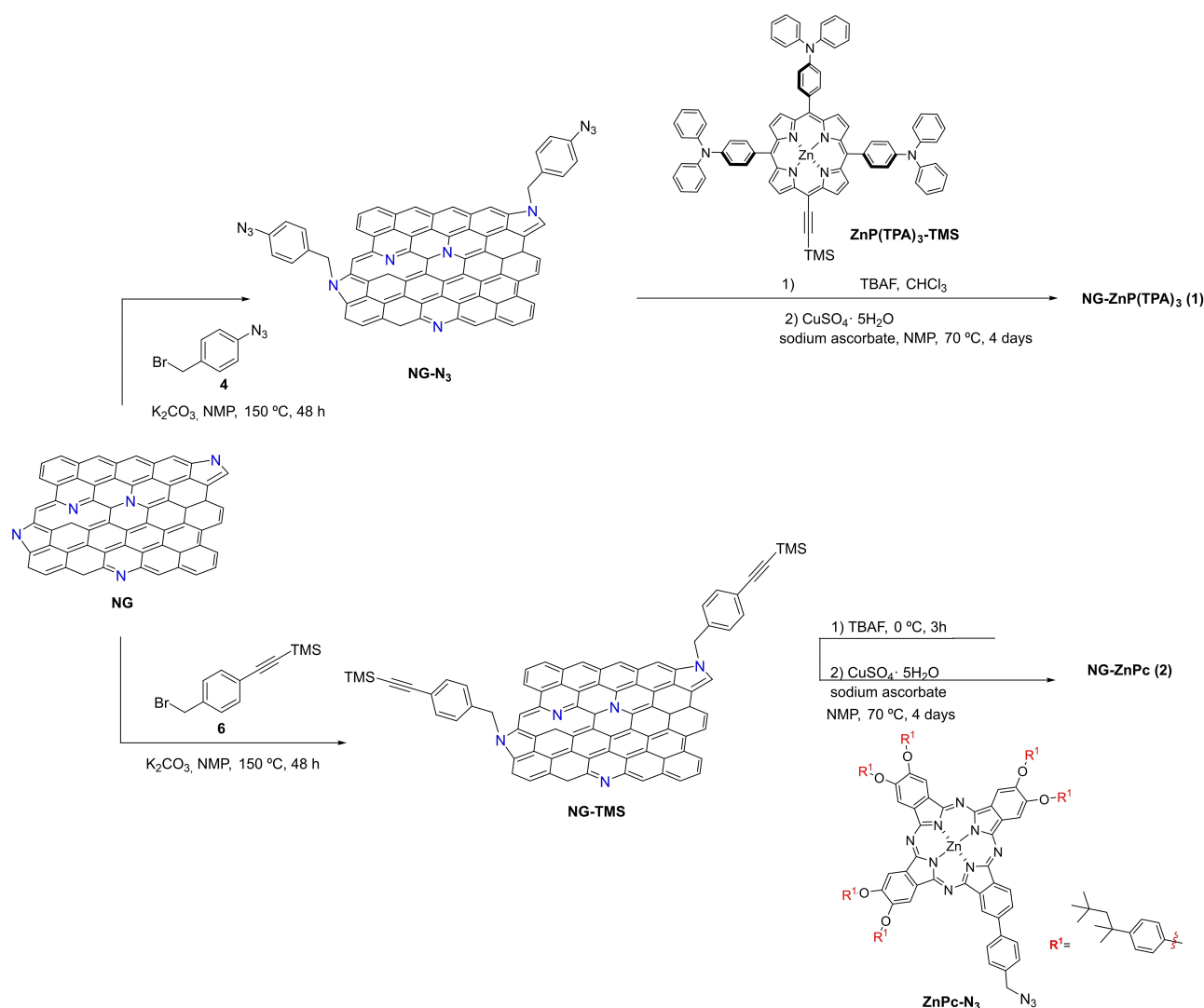**Figure 1.** Structures of the NG-functionalized materials, NG—ZnP(TPA)₃ (**1**) and NG—ZnPc (**2**), studied in the work.

Figure 2. a) Raman spectrum ($\lambda_{ex} = 532$ nm), b) AFM image and height profile, and c) TEM images for the starting NG material.

Chemistry–A European Journal

Research Article
doi.org/10.1002/chem.202200254

Chemistry Europe
European Chemical
Societies Publishing

We then attempted to functionalize this nitrogen-doped graphene (NG) as shown in Scheme 1. To that end, two different approaches were used. For hybrid **1**, exfoliated NG was initially treated with 1-azido-4-(bromomethyl) benzene (**4**; further details in the Supporting Information) in the presence of K_2CO_3[14] to obtain functionalized NG–N_3. Subsequently, ZnP(TPA)$_3$-TMS[21] was treated with TBAF to afford the deprotected porphyrin-bearing terminal alkyne subunits. The reaction of this deprotected porphyrin with NG–N_3 in NMP by Cu-catalyzed alkyne-azide cycloaddition (CuAAC)[22–25] afforded the desired material NG–ZnP(TPA)$_3$ (**1**). In the case of nanoconjugate **2**, *N*-alkylation of exfoliated NG with 4-(bromomethyl)phenylethynyl)trimethylsilane (**6**) was carried out at 150 °C for 4 days in the presence of K_2CO_3 to afford the corresponding NG-TMS. After deprotection of NG-TMS, the ethynylphenyl-functionalized conjugate was subjected to CuAAC conditions in NMP with ZnPc-N_3 to afford nanoconjugate **2** (Scheme 1). Synthesis of the new (azidomethyl)phenyl-substituted phthalocyanine (ZnPc-N_3) from ZnPc-CH_2OH is described in Scheme S1

in the Supporting Information. Briefly, ZnPc-CH_2OH was obtained following a synthetic route described by Sastre-Santos[26] that involves subjecting a mixture of 4-(*p*-hydroxymethylphenyl) phthalonitrile and 4,5-di(*tert*-octylphenoxy) phthalonitrile in a 1:3 molar ratio, to microwave irradiation. Subsequent bromination of the hydroxymethyl group with CBr_4 following the method described by Torres[27] gave the ZnPc–Br phthalocyanine in 85% yield, which was transformed into the ZnPc-N_3 azide derivative by treatment with excess sodium azide.

The new functionalized materials NG–ZnP(TPA)$_3$ and NG–ZnPc were characterized using a range of thermal, spectroscopic and microscopic techniques and compared with the starting NG sample, as outlined below.

First, TGA provides evidence that the cycloaddition reaction has taken place. Figures 3a and S1 show the TGA plots and first derivative curve (that indicates the temperature of the maximum in the weight loss rate of the material) for all materials synthesized along with those for the starting NG and photosensitizers for the sake of comparison. As can be seen in

Scheme 1. Preparation of NG derivatives **1** and **2** by click chemistry.
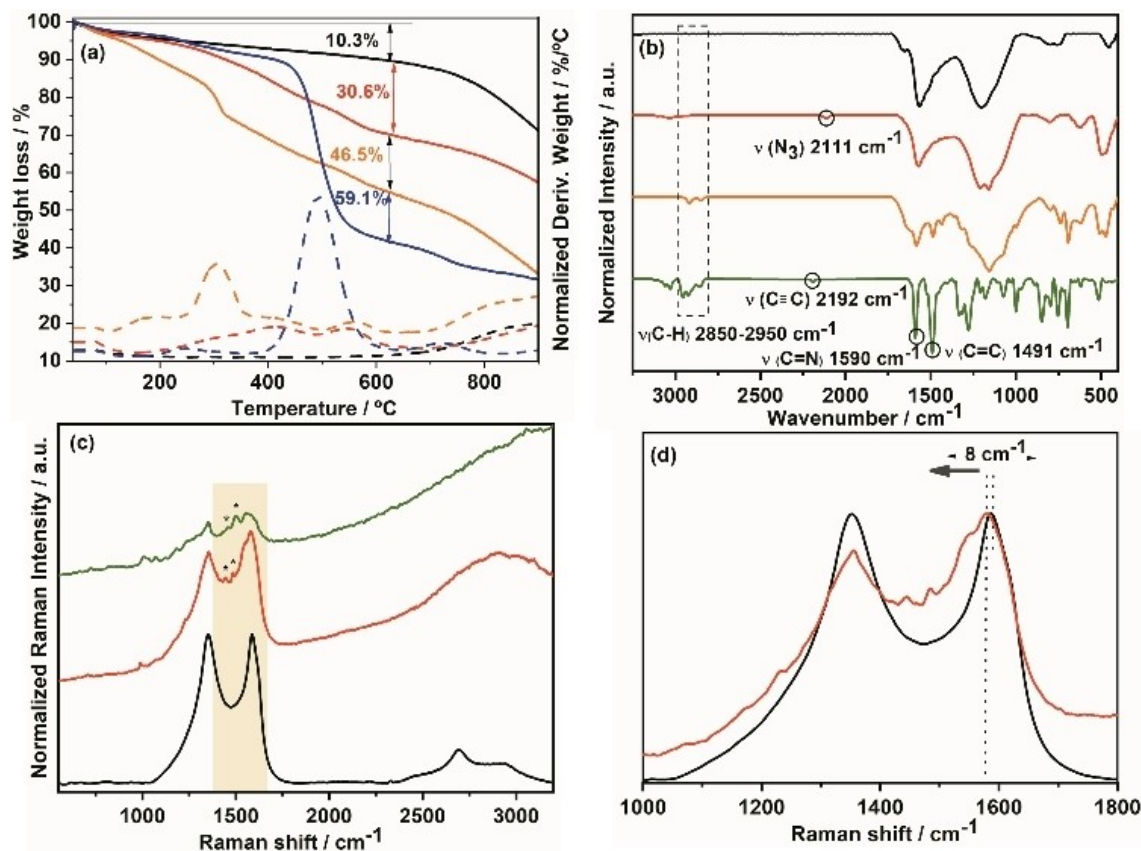
Chemistry–A European Journal

Research Article
doi.org/10.1002/chem.202200254

Chemistry Europe
European Chemical
Societies Publishing

Figure 3. a) TGA (solid lines) and first derivative curves (dashed lines; argon, 10 °C min^{-1}) of NG (——), NG—TMS (——), NG—ZnPc (——) and ZnPc (——). The TGA data for the starting material NG (——) are also provided for comparison. b) FTIR spectra of NG (——), NG—N$_3$ (——), NG—ZnP(TPA)$_3$ (——), and ZnP(TPA)$_3$ (——) showing suppression of the alkyne and azide vibrations in the final material. c) Superimposed Raman spectra (514 nm) for the starting NG (——), **1** (——), and ZnP(TPA)$_3$ (——). d) Expanded G-band region for NG (——) and functionalized NG—ZnP(TPA)$_3$ (——). The spectra are normalized to the intensity of the G mode to facilitate observation of the peak shift (8 cm^{-1}).

Figure 3a (for NG—ZnPc material), the thermogram of NG showed a weight loss of around 10.3%, attributed to defects in the starting material; TG analysis of NG-TMS showed a loss of 30.6%; lastly, NG—ZnPc displayed a weight loss of 46.5% (in a temperature range of 190–650 °C); the increase with respect to NG-TMS (15.9%) is directly related to the decomposition of the Zn—Pc moiety, being a direct indication of covalent anchoring, as a result of the success of the click reaction in the final material.

Further insight into the nature of the functionalized materials was obtained by FTIR spectroscopy (Figures 3b and S2). Thus, triazole ring formation after the click reaction was confirmed by the disappearance of the stretching vibration for the protected alkyne or the band assigned to the azide moiety.[22–28] As an example (Figure 3b), for the hybrid material decorated with zinc porphyrin (NG—ZnP(TPA)$_3$), no bands of protected alkyne and azide groups were observed. In contrast, new features attributed to skeletal deformation of the phenyl ring and the porphyrinoid macrocycle (C=C and C=N; 1456–1590 cm^{-1}) were observed, thus confirming the linkage between the organic moiety and the graphene surface.

Additional evidence for graphene functionalization came from structural characterization by means of Raman spectro-

scopy (514 nm; Figures 3c, d, S3 and S4). As mentioned above in Figure 2a, the Raman spectrum of NG displays the characteristic bands for these doped materials. Initial functionalization did not produce observable structural disorders (I_D/I_G). In addition, no differences were observed in the G band between the Raman spectrum for parent NG and those corresponding to the functionalized hybrids NG-TMS and NG—N$_3$, thus indicating a lack of change in the electronic state of the graphene sheet (Figure S4). When click coupling was performed, additional Raman peaks were detected, thus demonstrating incorporation of the electroactive moiety at the nitrogen-graphene surface. For instance, in the case of nanoconjugate **1** (Figure 3c), the new spectroscopic features observed were ascribed to the pyrrole rings and porphyrin core. Turning our attention to the G band of functionalized sample NG—ZnP(TPA)$_3$, this mode (~ 1579 cm^{-1}) is slightly downshifted with respect to the reference NG material (1587 cm^{-1}; Figure 3d), thereby suggesting the existence of N-doping[29] by ZnP(TPA)$_3$, as reported previously in the literature.[30]

To further investigate the functionalization of this material, we performed an X-ray photoelectron spectroscopy (XPS) study. The survey spectra recorded for all new conjugates display the electrons collected from the C1s, O1s, N1s, Si 2p and Zn 2p core

Chemistry–A European Journal

Research Article
doi.org/10.1002/chem.202200254

Chemistry
Europe
European Chemical
Societies Publishing

levels (Figures S5–S10, Tables S1 and S2). After initial functionalization by N-alkylation, the XPS survey spectra showed new contributions in the C1s and N1s core-level regions in comparison with the XPS spectrum of starting NG (Figure S5), thus supporting the covalent modification (Figures S6 and S7). The survey analysis for NG-TMS exhibited a weak Si 2p photoemission[15] (Figure S6) due to the TMS protective groups together with the presence of a new component at 285.5 eV due to the sp^3 C-atoms of the TMS units.[31] C 1s and N 1s components were also detected for the NG–N$_3$ derivative (Figure S7). Indeed, the expanded N 1s region (Figure S7c) revealed a clear contribution at 404 eV, which was assigned to the central electron-deficient nitrogen in the azido group. Although another component at around 401.5 eV was expected due to the differently charged nitrogen atoms in the azido unit, this signal was probably overlapped by the graphitic-type N already present in the starting NG material. After the second functionalization using the click reaction, several spectral changes were observed for both materials, **1** and **2** (Figures S10 and S11, Tables S1 and S2). Thus, in the N1s spectrum of materials for **1** and **2** (Figures S10b and S11c), the signal due to the azide group was absent and the signal arising from the triazole ring was buried beneath that for the pyrrolic-type N and graphitic-type N.[14] In addition, analysis of the high-resolution C1s core level of both nanoconjugates showed a change in the contribution at around 285.4 eV with respect to their precursors due to the sp^3 C atoms in the alkyl chains of the attached organic moieties (Figures S10a and S11b). Furthermore, both functionalized samples (**1** and **2**) showed a new peak at 1022 eV corresponding to Zn 2p$_{3/2}$, with binding energies close to those for bulk ZnPc and ZnP(TPA)$_3$, respectively (Figures S10c-S11e). These findings agree with the FTIR and Raman results and can be conclusive evidence for covalent grafting to the NG surface.

AFM measurements were performed to evaluate the morphology of the nanoconjugates (Figures 4 and S12). Dispersions of the different materials in ethanol were initially spin coated onto freshly cleaved mica surfaces and AFM images were acquired. The AFM images of the pristine NG material revealed the presence of few-layer graphene flakes (ca. 2–3 nm) with polygonal shape and well-defined edges (Figure 4a). Important to note that, after the introduction of the electro-active moieties, brightened zones were observed mainly at the edges of the flakes, which could be attributed to the presence of the electroactive moieties anchored to the graphene layers. However, the most notable observation was the change of flake morphology that occurred after the functionalization process, resulting in irregularly shaped graphene edges mainly consisting of rounded features (Figures 4b and S12a, b). The change in morphology was further confirmed by drop-casting the same dispersions onto mica surfaces. In this case, overlapped graphene layers were observable due to the drop-casting effect, but the morphological change of the edges was clearly evident (Figure S12c). Besides, the increase in heights observed in functionalized materials **1** and **2** are consistent with the theoretical distance calculated for the more stable conformations by DFT (Figure S13). These observations suggest anchoring of the organic moieties to the NG surface.

The electrochemical properties of both hybrids were also investigated. Figure S14 shows the differential pulse voltammograms (DPVs) for both hybrid materials in comparison with those for the reference compounds; the values obtained are collected in Table 1. These studies were performed at room temperature in *o*-dichlorobenzene/acetonitrile (*o*-DCB/AcCN 4:1, *v/v*) containing 0.1 M tetra-*N*-butylammonium hexafluorophosphate (TBAPF$_6$) as supporting electrolyte. The electrochemical data for nanohybrids **1** and **2** and the references compounds are provided in Table 1. In the anodic zone, nanoconjugate **1** displays three oxidation waves (+0.30, +0.53
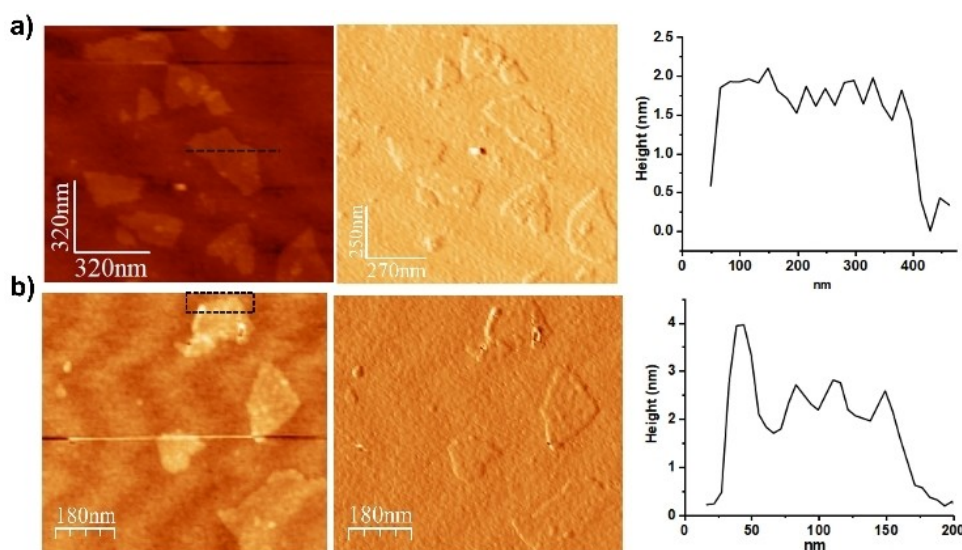

Figure 4. AFM topography (left), amplitude image (center), and height profile (right) for a) starting NG and b) functionalized NG–ZnPc **2** spin coated onto mica from ethanol dispersions.

Chemistry–A European Journal

Research Article
doi.org/10.1002/chem.202200254

Chemistry Europe
European Chemical
Societies Publishing

Table 1. Electrochemical data (V vs. Ag/AgNO₃) for all functionalized NG samples and precursors, determined by OSWV.[a]

Sample	E_{ox}^1 [V]	E_{ox}^2 [V]	E_{ox}^3 [V]	E_{ox}^4 [V]
ZnP(TPA)3-TMS	+0.26	+0.49	+0.71	+0.98
1	+0.30	+0.53	+0.79	–
ZnPc–N3	+0.25	+0.91	–	–
2	+0.32	+0.95	–	–

[a] Obtained in o-DCB/AcCN solution containing 0.1 M TBAPF₆ and using Ag/AgNO₃ as a reference electrode, glassy carbon as working electrode and a Pt wire counter electrode. Scan rate: 100 mV/s. Potentials are referenced to Fc/Fc⁺.

and +0.79 V), whereas derivative **2** exhibits two oxidation processes (+0.32 and +0.95 V), which can be clearly assigned to the oxidation of ZnP(TPA)₃-TMS (+0.26, +0.49, +0.71 and +0.98 V) and ZnPc-N₃ (+0.25 and +0.91 V) moieties. A comparison of these oxidation potentials shows a positive shift of 40 mV for nanoconjugate **1** and 70 mV in the case of **2** with respect to pristine ZnP(TPA)₃-TMS and ZnPc-N₃, respectively. Furthermore, hybrid **1** presents multi-electron oxidation due to the TPA moieties, as reported previously.[20,30] It may be mentioned here that due to the material nature of NG (instead of molecular type), Faradaic processes either in the cathodic

(reduction) or anodic (oxidation) potential scan was not observed.

The absorption and fluorescence spectrum for hybrids **1** and **2** are shown in Figure 5. The absorption spectrum for ZnP(TPA)₃-TMS displays a Soret band at 450 nm and Q bands at 562 and 612 nm.[20,33,34] In addition, the TPA entities result in a band with a maximum at 308 nm. The absorption band for NG is broad, covering the entire visible region, with a shoulder-type peak at 327 nm. For the NG–ZnP(TPA)₃ hybrid, the ZnP(TPA)₃-TMS bands show a blue-shift of 5–8 nm (443 nm for Soret, 558 and 606 nm for Q bands), with considerable broadening, thus indicating interactions between the porphyrin π-structure and the NG surface (Figure 5a). The flexible linkage connecting the NG and ZnP(TPA)₃ could facilitate such interactions. Similar observations were also found for **2**, with the original bands for ZnPc-N₃ located at 354, 620, and 689 nm being slightly blue-shifted to 345, 618, and 688 nm, respectively (Figure 5b). Additionally, the relatively large blue-shift of NG–ZnP(TPA)₃ hybrid compared to ZnP(TPA)₃- TMS could be due to converting meso-acetylene group of ZnP(TPA)₃ (π-extended structure) to meso-azide spacer group. The fluorescence spectrum of ZnP(TPA)₃ shows broadband with a maximum at 632 nm corresponding to the 0,0 transition, and a shoulder peak at 678 nm due to the 0,1 transition. In hybrid **1**, these bands were also found to be blue-shifted around ~15 nm and showed
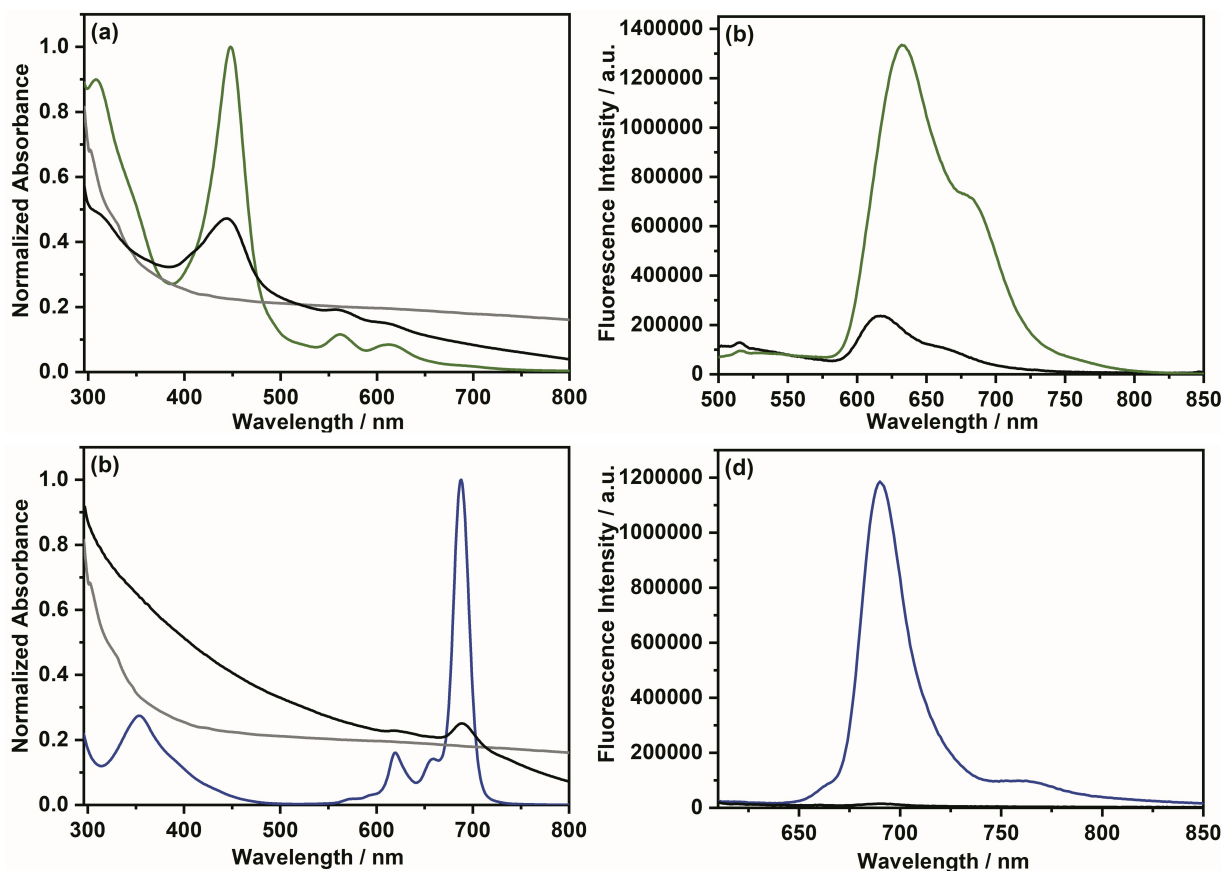

Figure 5. a), b) Absorption and c), d) fluorescence spectra of hybrid **1** (——) compared to NG (——) and ZnP(TPA)₃-TMS (—) and hybrid **2** (——) compared to NG (——) and ZnPc (—; equally absorbing) in DMF. ZnP(TPA)₃ was excited at 445 nm, whereas ZnPc was excited at 600 nm.

Chemistry–A European Journal

Research Article
doi.org/10.1002/chem.202200254

Chemistry Europe
European Chemical
Societies Publishing

significant quenching (over 88% of the initial intensity; Figure 5c). This quenching was found to be even more marked in the case of hybrid **2**. In this case, the ZnPc band located at 690 nm was quenched over 98% accompanied by a small blue-shift of 2 nm (Figure 5d). The lifetime ZnP(TPA)$_3$-TMS and ZnPc-N$_3$, as measured by time-correlated single-photon counting (TCSPC), were found to be 1.66 and 2.94 ns, respectively (Figure S15). For the hybrids, the decay was within the time resolution of our TCSPC setup which is less than 200 ps. These results suggest excited-state interactions between the singlet excited state of the photosensitizers and NG in the covalently linked hybrid.

The observed ZnP(TPA)$_3$ and ZnPc quenching in the hybrids can be explained by either static quenching due to the formation of non-fluorescent complexes, or excited energy transfer to NG or electron transfer from the singlet excited sensitizer to NG to yield charge-transfer products. Although quenching due to non-fluorescent complex formation and excited energy transfer cannot be fully ruled out as contributing factors, the facile oxidation of ZnP(TPA)$_3$ and ZnPc suggests electron transfer could be a possible mechanism for fluorescence quenching. Mechanistically, the odd electron from the LUMO level of the excited state probe could transfer to a low-lying conduction band in NG to produce NG$^{\bullet-}$-ZnP(TPA)$_3{}^{\bullet+}$ and NG$^{\bullet-}$-ZnPc$^{\bullet+}$ electron-transfer products. To characterize the products of electron transfer spectrally, the photosensitizers were oxidized either electrochemically or chemically and their spectra were recorded. Figures S16a and b show the spectral changes observed for ZnP(TPA)$_3$-control and ZnPc-control during the oxidation process. New peaks in the 475 nm range (broad shoulder to the Soret band) and broad absorption covering the range 625–825 nm, with a maximum at 775 nm, were observed for ZnP(TPA)$_3{}^+$-control.

Femtosecond transient absorption (fs-TA) spectral studies were performed in DMF as the solubility of the hybrids in this solvent was found to be reasonable. Figure 6a shows fs-TA spectra at the indicated delay times for ZnP(TPA)$_3$-control at the Soret band excitation. The ^{1}ZnP(TPA)$_3$*-control species formed immediately after excitation (see spectrum at 1.8 ps) revealed excited state absorption (ESA) peaks at 496, 535 (shoulder band), 588, 727, and 774 nm in the visible spectral region. This was accompanied by negative peaks at 568 and 626 nm due to ground state bleaching (GSB) and stimulated emission (SE). Slow decay and recovery of the positive and negative peaks (see Figure 6b(i) for a time profile of ^{1}ZnP(TPA)$_3$*-control) was complemented by the slow growth of a new peak at 485 nm
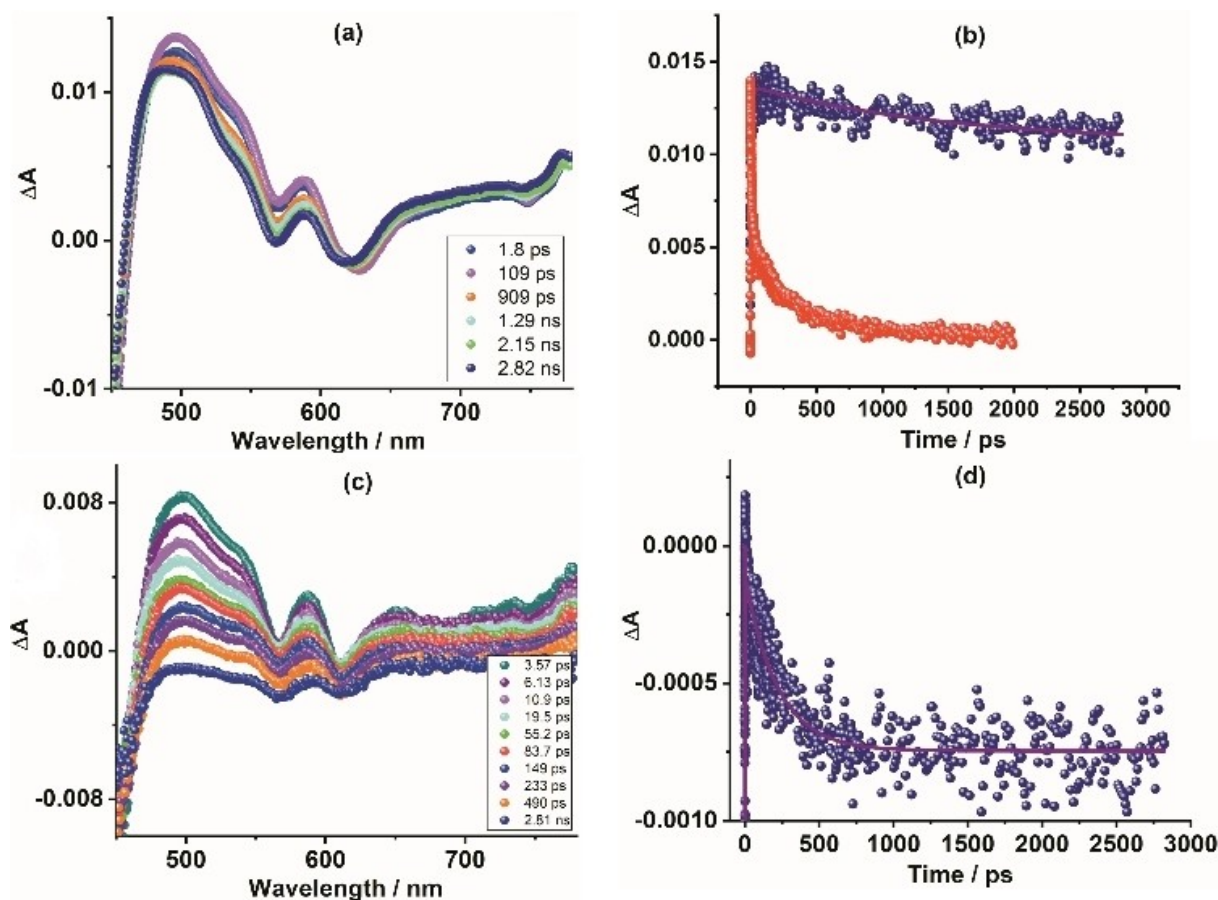

Figure 6. Fs-TA spectra at indicated delay times for a) the ZnP(TPA)$_3$-control and c) hybrid **1** in DMF at an excitation wavelength of 425 nm with 100 fs laser pulses. b) Time profile for i) the ^{1}ZnP(TPA)$_3$*-control at 495 nm and ii) **1** at 498 nm corresponding to ^{1}ZnP(TPA)$_3$.* d) Time profile for the 650 nm peak corresponding to ZnP(TPA)$_3{}^+$

Chemistry–A European Journal

Research Article
doi.org/10.1002/chem.202200254

Chemistry Europe
European Chemical
Societies Publishing

and a broad peak with a maximum at 774 nm. The assignment of these news peaks to ^{3}ZnP(TPA)$_3$*-control was confirmed by nanosecond transient absorption spectroscopy, as shown in Figure S17a. ^{3}ZnP(TPA)$_3$*-control decayed with a time constant of 16.8 μs. Interestingly, in the case of the NG–ZnP(TPA)$_3$ hybrid (1), relaxation of the ^{1}ZnP(TPA)$_3$* peaks was rather rapid, (see Figure 6b(ii) for the time profile of NG–^{1}ZnP(TPA)$_3$*), with no indication of the formation of ^{3}ZnP(TPA)$_3$* However, a new broad peak, corresponding to ZnP(TPA)$_3$$^{•+}$ appeared in the range 625–775 nm (Figure 6c), thus providing experimental evidence for charge separation in hybrid 1. The rate constants for charge separation (k_{CS}) and charge recombination (k_{CR}), as measured using the growth and decay monitored at 650 nm, were found to be approximately ~10^{10} and 4.56×10^9 s^{-1} respectively (see Figure 6d for the time profile). Diluting the hybrid solutions approximately to half of the initial concentration resulted in similar k_{CS} and k_{CR} values indicating the observed photo-events are intramolecular (involving covalently linked sensitizer-NG) as against intermolecular.

The Fs-TA spectrum for ZnPc-control at the indicated delay times is shown in Figure 7a. In the visible region, ^{1}ZnPc*-control is characterized by ESA peaks at 482, 594, 635, and 736 nm. Similarly, peaks at 612 and 685 nm due to GSB and SE,

respectively, are also observed. The decay and recovery of the positive and negative peaks was slow (see Figure 7b for time profile of 736 nm), which is consistent with a longer lifetime for ^{1}ZnPc*-control, and a new peak can be seen at 510 nm. Ns-TA spectral studies confirmed that this peak is due to ^{3}ZnPc,* as shown in Figure S17b, with a lifetime for ^{3}ZnPc*-control of about 4.5 μs. In the case of NG–ZnPc (2), the transient spectrum recorded at 2.51 ps was markedly different from that observed for ^{3}ZnPc*-control. Thus, at decay times of less than 2.51 ps, the spectrum (not shown) is structureless perhaps due to rapid vibrational cooling and solvent relaxation. In any case, the 2.51 ps spectrum revealed the main ESA peak at 557 nm (Figure 7c), which agrees well with the value for ZnPc$^{•+}$ obtained by chemical oxidation (Figure S16b). Interestingly, no signal 480 nm due to ESA or at 612 nm due to GSB for ^{1}ZnPc* was observed, thus indicating completion of the charge-separation process in less than 2.5 ps. The k_{CS} and k_{CR} values for the growth and decay monitored at 557 nm, were found to be $> 10^{10}$ and 1.64×10^9 s^{-1}, respectively (see Figure 7d for the time profile). These results confirm successful excited-state charge separation in both 1 and 2.[36,37]
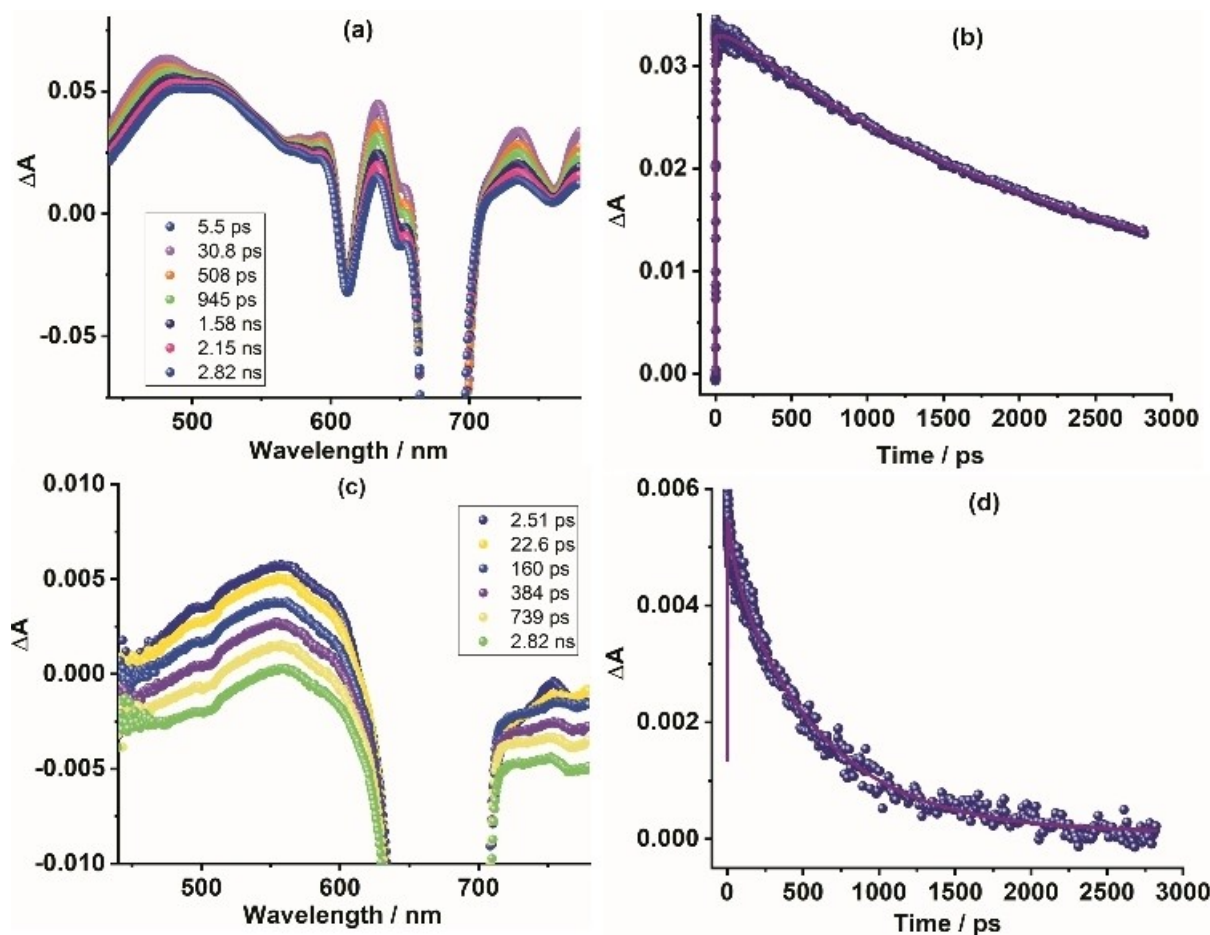

Figure 7. Fs-TA spectra at indicated delay times for a) ZnPc-control and c) hybrid 2 in DMF at an excitation wavelength of 684 nm with 100 fs laser pulses. b) Time profile for ^{1}ZnPc*-control at 736 nm. d) Time profile for 557 nm peak corresponding to ZnPc$^+$.

Conclusion

By using a click chemistry reaction, N-doped graphene has been successfully grafted with two well-known photosensitizers, namely zinc porphyrin and zinc phthalocyanine. Systematic spectroscopic, thermogravimetric, and imaging studies have been performed to establish the degree of covalent grafting in the resulting NG–ZnP and NG–ZnPc hybrids. Fluorescence of both ZnP and ZnPc in these hybrids was found to be significantly quenched, and their facile oxidation supported the electron-transfer quenching mechanism. Subsequent femtosecond transient-absorption spectral studies provided proof for the charge-separation process. The measured rates of charge separation and recombination were of the order of 10^{10} and 10^9 s^{-1}, respectively, thereby suggesting efficient electron-transfer events. Further studies to stabilize the charge-separated states by using a multimodular covalent-grafting approach are in progress in our laboratories.

Experimental Section

Chemicals: Nitrogen-doped graphene (NG, grade TNNRGO) was supplied by Chengdu Organic Chemicals Co. Ltd., Chinese Academy of Sciences (Chengdu, P. R. China; (www.timesnano.com). Starting NG material presents a nitrogen content of 5–10 wt% (grade TNNRGO). The synthesis and characterization of ZnP(TPA)$_3$, ZnPc-N$_3$ and compounds **4** and **6** was described in detail in the Supporting Information. For the exfoliation procedure, NG material (1 mg) was dispersed in NMP (3 mL) at room temperature using a sonicator bath at low power (37 kHz) for 30 min. After that, the resulting dispersion was centrifuged for 10 min at 500 rpm; the supernatant was separated and stored in solution. The concentration in the resulting dispersion was determined from the absorbance at 660 nm by using the Lambert-Beer law. All manipulations were carried out under dry argon atmosphere by using standard Schlenck-type techniques. Organic solvents and reagents used in this work were purchased from commercial suppliers and used as received unless otherwise stated. Thin-layer chromatography (TLC) was performed on aluminium-coated Merck Kieselgel 60 F254 plates to check the progress of the reactions, and chromatograms were visualized with UV light ($\lambda = 254$ and 360 nm). Column chromatography was performed on Merck silica gel 60 (ASTM 230–400 mesh).

Instrumentation: Bath sonicator Elmasonic P at 37 MHz, 100% power was used for preparing graphene dispersions. NMR spectra were recorded with a Bruker AC 300 and a Bruker TopSpin AV-400 spectrometer. Chemical shifts are reported in delta (δ) units, expressed in parts per million (ppm) downfield from tetramethylsilane (TMS) with residual protonated solvent as an internal standard (CDCl$_3$, 7.26 ppm).

FTIR spectra were carried out in a Fourier Transform IR spectrophotometer (Avatar 370) using a spectral range of 4000–400 cm^{-1}, with a resolution of 1 cm^{-1} and in pellets of dispersed samples of the corresponding materials in dried KBr. Mass spectra were obtained from a Bruker Microflex matrix-assisted laser desorption/ionization time of flight (MALDI-TOF) and from a VOYAGER DETM STR mass spectrometer (MALDI-TOF) using dithranol as matrix.

Thermogravimetric analyses (TGA) were performed using a TGA/DSC Linea Excellent instrument by Mettler-Toledo, collected under a flow of nitrogen (90 mL.min^{-1}). The sample (~0.5 mg) was introduced inside a platinum crucible and equilibrated at 40 °C followed by a 10 °C min^{-1} ramp between 40 and 1000 °C. The weight changes were recorded as a function of temperature.

Raman spectra were recorded on a Renishaw inVia Raman instrument coupled with a Leica microscope at room temperature with a 514 nm exciting laser. The samples were deposited on SiO$_2$ wafers. Measurements were taken with 10 s of exposure times at varying numbers of accumulations. Raman spectra images are an average of 1000 points. The laser spot was focused on the sample surface using a long working distance 100× objective. Raman spectra were collected on numerous spots on the sample and recorded with a Peltier cooled CCD camera. The intensity ratio I_D/I_G was obtained by taking the peak intensities following any baseline corrections. The data were collected and analyzed with Renishaw Wire and Origin software.

Steady-state absorption spectra was recorded with a Jasco V-670 and Shimadzu UV 3600 spectrophotometers. Steady-state fluorescence spectra and fluorescence lifetime were evaluated by using a Cary Eclipse fluorescence spectrophotometer or a Horiba Yvon Nanolog spectrofluorometer equipped with PMT (for UV-visible) and InGaAs (for near-IR) detectors. The fluorescence lifetimes were measured with the Time Correlated Single Photon Counting (TCSPC) option with nano-LED excitation source ($\lambda_{ex} = 494$ nm) on the Nanolog. All the solutions were purged prior to spectral measurements using argon gas.

AFM images were recorded in tapping mode using a Multimode 8 system (Veeco Instruments Inc., Santa Barbara, USA) with a Nano-Scope V controller (Digital Instruments, Santa Barbara, USA) operating at room temperature in ambient air conditions. RTESP-300 Bruker silicon cantilevers with a resonance frequency of 300 kHz and a nominal force constant of 40 N m^{-1} were used for AFM measurements. The images were processed using WSxM1 (freely downloadable scanning probe microscopy software from www.wsxmsolutions.com). The samples were prepared drop-casting onto a silicon wafer using a dispersion of the different samples (0.5 mg mL^{-1}) in MilliQ aqueous solution containing 2 wt% sodium dodecylbenzene sulfonate (SDBS). The samples were prepared using freshly cleaved mica surfaces, on which dispersions of the different materials in ethanol (0.5 mg m.L^{-1}) were spin coated (Figures 4 and S12 a) or drop casted (Figure S12 b).

XPS analysis was obtained using an Escalab 200R (VG, UK) electron spectrometer equipped with a hemispherical analyzer, operating in the constant pass energy mode, and an Mg$_{K\alpha}$ ($h\nu = 1253.6$ eV, 1 eV $= 1.603 \times 10-19$ J) X-ray source operated at 10 mA and 12 kV. The detection angle of photoelectrons was 60° to the surface of the specimen. The spectrometer was calibrated against Au 4f$_{7/2}$ line at 84.0 eV using a gold sheet and Cu 2p$_{3/2}$ at 932.5 eV from a copper sheet. Charge effects on the samples were removed by taking the C 1s line from adventitious carbon at 284.8 eV. To estimate the photoelectron peak intensities, the background was subtracted from the measured spectra according to the Shirley method and using a combination of Gaussian and Lorentzian lines (90G–10L) using the software "XPS peak". All elemental concentrations were calculated using the relative sensitivity factors specific to the spectrometer. The elemental concentrations in atomic percent (at %) for the different elements were calculated using the recorded high-resolution spectra. The reproducibility of the results was confirmed several times under the same conditions.

Osteryoung square wave voltammetry (OSWV) was performed in ODCB/Acetonitrile 4:1 solution. Tetrabutylammonium hexafluorophosphate (TBAPF$_6$; 0.1 M as supporting electrolyte) was purchased from Aldrich-Sigma and used without purification. Solutions were deoxygenated by argon bubbling prior to each experiment, which

was run under argon atmosphere. Experiments were done in a one-compartment cell equipped with a platinum working microelectrode ($\emptyset = 2$ mm) and a platinum wire counter electrode. A scan rate of $0.1\,V\,s^{-1}$ was used. An $Ag/AgNO_3$ electrode was used as reference and checked against the ferrocene/ferrocenium couple (Fc/Fc^+) before and after each experiment.

Femtosecond transient absorption spectroscopy experiments were carried out using an ultrafast femtosecond laser source (Libra) by Coherent incorporating diode-pumped, mode locked Ti:Sapphire laser (Vitesse) and diode-pumped intra cavity doubled Nd:YLF laser (Evolution) to generate a compressed laser output of 1.45 W. For optical detection, a Helios transient absorption spectrometer coupled with femtosecond harmonics generator both provided by Ultrafast Systems LLC was used. The source for the pump and probe pulses were derived from the fundamental output of Libra (Compressed output 1.45 W, pulse width 100 fs) at a repetition rate of 1 kHz. 95% of the fundamental output of the laser was introduced into a TOPAS-Prime-OPA system with 290–2600 nm tuning range from Altos Photonics Inc., (Bozeman, MT), while the rest of the output was used for generation of white light continuum. Kinetic traces at appropriate wavelengths were assembled from the time-resolved spectral data. Data analysis was performed using Surface Xplorer software supplied by Ultrafast Systems. All measurements were conducted in degassed solutions at 298 K.

Acknowledgments

Conflict of Interest

The authors declare no conflict of interest.

Data Availability Statement

The data that support the findings of this study are available in the supplementary material of this article.

[1] S. Nasir, M. Z. Hussein, Z. Zainal, N. A. Yusof, *Materials* **2018**, *11*, 295–319.
[2] V. Georgakilas, J. A. Perman, J. Tucek, R. Zboril, *Chem. Rev.* **2015**, *115*, 4744–4822.
[3] Z. Li, Z. Liu, H. Sun, C. Gao, *Chem. Rev.* **2015**, *115*, 7046–7117.
[4] G. Bottari, M. Ángeles Herranz, L. Wibmer, M. Volland, L. Rodríguez-Pérez, D. M. Guldi, A. Hirsch, N. Martín, F. D'Souza, T. Torres, *Chem. Soc. Rev.* **2017**, *46*, 4464–4500.
[5] O. Ito, *Chem. Rec.* **2017**, *17*, 326–362.
[6] F. D'Souza, O. Ito, *Chem. Soc. Rev.* **2012**, *41*, 86–96.
[7] V. Sgobba, D. M. Guldi, *Chem. Soc. Rev.* **2009**, *38*, 165–184.
[8] G. Bottari, G. de La Torre, D. M. Guldi, T. Torres, *Chem. Rev.* **2010**, *110*, 6768–6816.
[9] D. Jariwala, V. K. Sangwan, L. J. Lauhon, T. J. Marks, M. C. Hersam, *Chem. Soc. Rev.* **2013**, *42*, 2824–2860.
[10] T. Umeyama, H. Imahori, *J. Phys. Chem. C* **2013**, *117*, 3195–3209.
[11] T. Umeyama, H. Imahori, *Nanoscale Horiz.* **2018**, *3*, 352–366.
[12] H. Wang, T. Maiyalagan, X. Wang, *ACS Catal.* **2012**, *2*, 781–794.
[13] M. Barrejón, A. Primo, M. J. Gómez-Escalonilla, J. L. García-Fierro, H. García, F. Langa, *Chem. Commun.* **2015**, *51*, 16916–16919.
[14] M. Barrejón, L. M. Arellano, H. B. Gobeze, M. J. Gómez-Escalonilla, J. L. García-Fierro, F. D'Souza, F. Langa, *Chem. Sci.* **2018**, *9*, 8221–8227.
[15] H. B. Gobeze, L. M. Arellano, A. M. Gutiérrez-Vílchez, M. J. Gómez-Escalonilla, Á. Sastre-Santos, F. Fernández-Lázaro, F. Langa, F. D'Souza, *Nanoscale Adv.* **2019**, *1*, 4009–4015.
[16] C. Hu, D. Liu, Y. Xiao, L. Dai, *Prog. Nat. Sci.* **2018**, *28*, 121–132.
[17] J.-H. Chou, M. E. Kosal, H. S. Nalwa, N. A. Rakow, K. S. Suslick in, *The Porphyrin Handbook* (Eds.: K. M. Kadish, K. M. Smith, R. Guilard) Academic Press, New York, **2000**, p. 43.
[18] G. de La Torre, C. G. Claessens, T. Torres, *Chem. Commun.* **2007**, 2000–2015.
[19] J. Mack, N. Kobayashi, *Chem. Rev.* **2011**, *111*, 281–321.
[20] L. M. Arellano, M. Barrejón, H. B. Gobeze, M. J. Gómez-Escalonilla, J. L. García-Fierro, F. D'Souza, F. Langa, *Nanoscale* **2017**, *9*, 7551–7558.
[21] A. Aljarilla, J. N. Clifford, L. Pellejà, A. Moncho, S. Arrechea, P. D. la Cruz, F. Langa, E. Palomares, *J. Mater. Chem. A* **2013**, *1*, 13640–13647.
[22] M. Barrejón, M. Vizuete, M. J. Gómez-Escalonilla, J. L. García-Fierro, I. Berlanga, F. Zamora, G. Abellán, P. Atienzar, J. F. Nierengarten, H. García, F. Langa, *Chem. Commun.* **2014**, *50*, 9053–9055.
[23] M. Vizuete, M. J. Gómez-Escalonilla, J. L. García-Fierro, M. Yudasaka, S. Iijima, M. Vartanian, J. Iehl, J. F. Nierengarten, F. Langa, *Chem. Commun.* **2011**, *47*, 12771–12773.
[24] M. Vizuete, M. J. Gómez-Escalonilla, J. L. García-Fierro, A. S. D. Sandanayaka, T. Hasobe, M. Yudasaka, S. Iijima, O. Ito, F. Langa, *Chem. Eur. J.* **2010**, *16*, 10752–10763.
[25] J. Mateos-Gil, L. Rodríguez-Pérez, M. Moreno Oliva, G. Katsukis, C. Romero-Nieto, M. Á. Herranz, D. M. Guldi, N. Martín, *Nanoscale* **2015**, *7*, 1193–1200.
[26] L. Martín-Gomis, C. Parejo, J. C. Álvarez, F. Fernández-Lázaro, Á. Sastre-Santos, *Inorg. Chim. Acta* **2017**, *468*, 327–333.
[27] B. J. Campo, J. Duchateau, C. R. Ganivet, B. Ballesteros, J. Gilot, M. M. Wienk, W. D. Oosterbaan, L. Lutsen, T. J. Cleij, G. de La Torre, R. A. J. Janssen, D. Vanderzande, T. Torres, *Dalton Trans.* **2011**, *40*, 3979–3988.
[28] L. Rodríguez-Pérez, J. Ramos-Soriano, A. Pérez-Sánchez, B. M. Illescas, A. Muñoz, J. Luczkowiak, F. Lasala, J. Rojo, R. Delgado, N. Martín, *J. Am. Chem. Soc.* **2018**, *140*, 9891–9898.
[29] H. J. Shin, M. K. Soo, S. M. Yoon, A. Benayad, K. K. Ki, J. K. Sung, K. P. Hyun, J. Y. Choi, H. L. Young, *J. Am. Chem. Soc.* **2008**, *130*, 2062–2066.
[30] L. M. Arellano, H. B. Gobeze, M. J. Gómez-Escalonilla, J. L. García-Fierro, F. D'Souza, F. Langa, *Nanoscale* **2020**, *12*, 9890–9898.
[31] L. M. Arellano, L. Martín-Gomis, H. B. Gobeze, D. Molina, C. Hermosa, M. J. Gómez-Escalonilla, J. L. García-Fierro, Á. Sastre-Santos, F. D'Souza, F. Langa, *Nanoscale* **2018**, *10*, 5205–5213.
[32] J. P. Collman, N. K. Devaraj, T. P. A. Eberspacher, C. E. D. Chidsey, *Langmuir* **2006**, *22*, 2457–2464.
[33] C. B. Kc, G. N. Lim, F. D'Souza, *Nanoscale* **2015**, *7*, 6813–6826.
[34] F. D'Souza, S. Gadde, D. M. Shafiqul Islam, C. A. Wijesinghe, A. L. Schumacher, M. E. Zandler, Y. Araki, O. Ito, *J. Phys. Chem. A* **2007**, *111*, 8552–8560.
[35] S. K. Das, A. Mahler, A. K. Wilson, F. D'Souza, *ChemPhysChem* **2014**, *15*, 2462–2472.
[36] M. Barrejón, L. M. Arellano, F. D'Souza, F. Langa, *Nanoscale* **2019**, *11*, 14978–14992.
[37] M. Barrejón, H. B. Gobeze, M. J. Gómez-Escalonilla, J. L. García-Fierro, M. Zhang, M. Yudasaka, S. Iijima, F. D'Souza, F. Langa, *Nanoscale* **2016**, *8*, 14716–14724.